

REPORT DOCUMENTATION PAGE		READ INSTRUCTIONS BEFORE COMPLETING FORM
1. REPORT NUMBER NRL Report 7853	2. GOVT ACCESSION NO.	3. RECIPIENT'S CATALOG NUMBER
4. TITLE (and Subtitle) X-RAY LINE PROFILE ANALYSIS OF TITANIUM ALLOYS		5. TYPE OF REPORT & PERIOD COVERED Final report on one phase of the NRL Problem.
		6. PERFORMING ORG. REPORT NUMBER
7. AUTHOR(s) E.A. Metzbower		8. CONTRACT OR GRANT NUMBER(s)
9. PERFORMING ORGANIZATION NAME AND ADDRESS Naval Research Laboratory Washington, D.C. 20375		10. PROGRAM ELEMENT, PROJECT, TASK AREA & WORK UNIT NUMBERS NRL Problem M01-08 Project RR 022-01-46
11. CONTROLLING OFFICE NAME AND ADDRESS Office of Naval Research 800 North Quincy Street Arlington, VA. 22217		12. REPORT DATE February 4, 1975
		13. NUMBER OF PAGES 18
14. MONITORING AGENCY NAME & ADDRESS (if different from Controlling Office)		15. SECURITY CLASS. (of this report) Unclassified
		15a. DECLASSIFICATION/DOWNGRADING SCHEDULE
16. DISTRIBUTION STATEMENT (of this Report) Approved for public release; distribution unlimited.		
17. DISTRIBUTION STATEMENT (of the abstract entered in Block 20, if different from Report)		
18. SUPPLEMENTARY NOTES		
19. KEY WORDS (Continue on reverse side if necessary and identify by block number) X-ray X-ray analysis Titanium alloys Dislocations <u>Short-range order Stacking faults</u>		
20. ABSTRACT (Continue on reverse side if necessary and identify by block number) X-ray-line-profile analysis has been used to investigate the dislocation structures resulting from severe plastic deformation in a series of titanium alloys. The effect of oxygen level (up to 0.33 wt-%) on the dislocation arrangements in titanium as well as in a series of titanium-aluminum alloys (4, 6, and 9 wt-% Al) was the principal thrust of the investigation. Four commercial alpha-phase titanium alloys (Ti-7Al-2Cb-1Ta, Ti-5Al-2.5 Sn, Ti-7Al-12 Zr, and Ti-4Al-3Mo-1V) were also examined. Although correlations were found between the stacking fault probability and alloying elements, the dislocation arrangements can not be interpreted (continued)		

(block 20 continued)

solely in terms of stacking fault energies. Short-range order definitely plays an important role, and solute-dislocation interactions may be active.

CONTENTS

INTRODUCTION	1
DISLOCATION ARRANGEMENTS	2
X-RAY-LINE-BROADENING PROCEDURES	6
FOURIER ANALYSIS	7
EXPERIMENTAL RESULTS	8
DISCUSSION	9
Ti-O Alloys	10
Ti-Al-O Alloys	11
Ti-6Al-4V-Oxygen Alloys	12
Commercial Ti Alloys	13
CONCLUSIONS	14
REFERENCES	14

X-RAY LINE PROFILE ANALYSIS OF TITANIUM ALLOYS

INTRODUCTION

Information concerning the small coherent domains, the microstrains, and stacking faults within these domains, can be extracted from analyzing the x-ray line shapes of cold worked metals and alloys. This classification of features is made only for convenience in x-ray analysis, since these features are a manifestation of the dislocation substructures of deformed metals and alloys. Cold-worked face-centered-cubic metals and alloys have been the object of most x-ray-line-broadening studies, and the incidence of stacking faults in these alloys has been thoroughly studied and useful information thus obtained. The correlations between dislocation theory and x-ray line broadening have been excellent for the face-centered-cubic metals and alloys. Similar data in body-centered-cubic and hexagonal-close-packed metals and alloys are relatively lacking.

The α and $\alpha + \beta$ phase titanium alloys for the most part have been designed around the binary Ti-Al solid-solution alloys. The solid solubility of aluminum in titanium extends up to about 12 at-% at room temperature, whereas at elevated temperatures the $\alpha + \beta$ phase field is opened up and the $\alpha \rightleftharpoons \beta$ transformation temperature is effectively raised. The yield strength of a Ti-10-at-%-Al alloy is about 3.5 times greater than the yield strength of pure titanium. Electron microscopy of α titanium alloys has shown that as the aluminum content increases, the dislocation arrangements change from a three-dimensional cellular structure to a two-dimensional planar structure. Electron microscopy of these alloys also suggests that they have a rather high stacking-fault energy, since the nodes do not separate sufficiently to permit measurements. In such cases the x-ray-line-broadening method becomes a particularly relevant technique for the investigation of faulting.

Detailed measurements of x-ray line broadening of binary Ti-Al alloys have been previously reported [1, 2]. The object of the present investigation was to measure the x-ray line broadening of commercial titanium alloys and to interpret these results in terms of the binary Ti-Al alloys. Materials studied were three titanium-aluminum alloys (4, 6, and 9 wt-% aluminum), each with two or three oxygen contents (near 0.08, 0.15, and 0.33 wt-%); three pure titanium specimens, each with a different oxygen level (0.01, 0.12 and 0.3 wt-%); three Ti-6Al-4V specimens, each with a different oxygen level (0.05, 0.11, and 0.15 wt-%); and four commercially available titanium alloys (Ti-7Al-2Cb-1Ta, Ti-5Al-2.5Sn, Ti-7Al-12Zr, and Ti-4Al-3Mo-1V). Transmission electron microscopy was used to correlate these data with measurements of the stacking fault probability.

Note: Manuscript submitted December 10, 1974.

DISLOCATION ARRANGEMENTS

The examination of thin foils of α Ti-Al alloys by transmission electron microscopy has shown that in the alloys with low (≤ 5 wt-%) Al content the dislocation arrangement is cellular (three-dimensional) (Fig. 1a) whereas in the alloys with higher (≤ 6 wt-%) Al content the dislocation arrangement becomes planar (two-dimensional) (Fig. 1b). Studies of stress corrosion cracking (SCC) indicate that in seawater the alloys with low Al content are nonsusceptible whereas the alloys with higher Al content are susceptible.

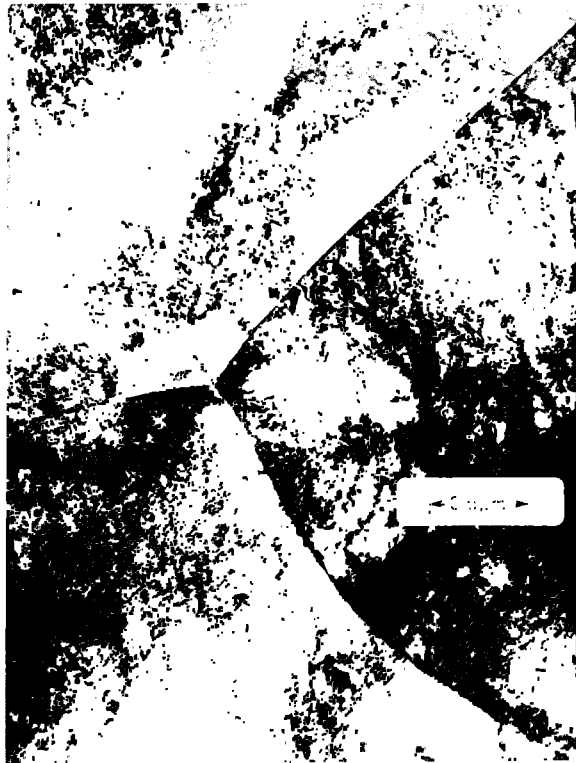


Fig. 1a — Transmission electron micrograph of a Ti-2-wt-%-Al alloy, showing a cellular dislocation structure

Susceptibility to SCC and the dislocation arrangements found in these α Ti alloys are thus correlated. Two fundamental questions remain: the cause of the change in dislocation arrangements with alloying, and how the dislocation arrangements affect the susceptibility of these alloys to SCC. We shall address ourselves to the first question by

attempting to deduce why the dislocation arrangements change with alloying and by measuring a physical quantity which can be related to these changes.

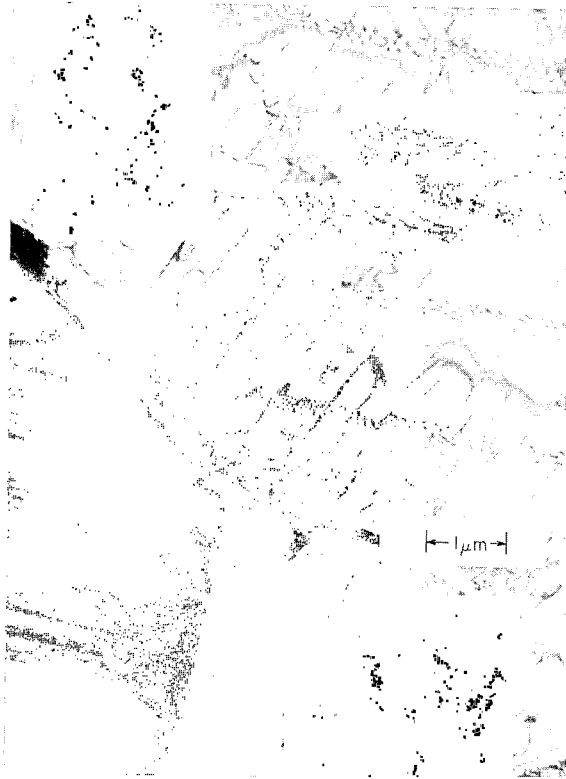


Fig. 1b — Transmission electron micrograph of a Ti-7.75-wt-%-Al alloy, showing a planar dislocation structure

The ease of cross-slip is known to affect the dislocation arrangements in deformed metals [3, 4]. The ease of cross-slip allows the dislocations to glide from one set of a family of slip planes onto another; thus a cellular structure develops. Easy cross-slip is usually associated with the formation of dislocation dipoles, debris, Frank loops, and stacking-fault tetrahedra. Difficult cross-slip implies that the locations are constrained to a series of parallel slip planes; thus a planar structure develops. Multipole formation and the absence of Frank loops and tetrahedra are other indications of the lack of cross-slip.

The ability of an alloy to cross-slip usually is thought to depend on one of three factors: the stacking fault energy (γ), dislocation-solute interactions, and short-range order. If cross-slip takes place by means of the constriction of a stacking fault, then cross-slip depends on γ . In hexagonal-close-packed metals perfect dislocations

with Burgers vectors of the type $(a/3)\langle 11\bar{2}0 \rangle$ (energy $\approx a^2$) may dissociate in the basal plane into two low-energy Shockley partial dislocations of the type $(a/3)\langle 10\bar{1}0 \rangle$ (energy $\approx a^2/3$) surrounding an intrinsic stacking fault. The dissociated dislocation is restricted to slip in the basal plane, but constriction of screw segments will enable cross-slip to occur on $\{10\bar{1}n\}$ planes [5]. Any given $\{10\bar{1}n\}$ plane can contain only one of three possible $\pm \{11\bar{2}0\}$ Burgers vectors. Energetically this dissociation is favorable; thus this is a possible mechanism for cross-slip, depending on the value of the stacking fault energy γ . That is, if γ is high, dissociation will occur, whereas if γ is low, the dislocations will not dissociate. Cross-slip then will be aided by a high γ , but will be impeded by a low γ .

Dislocation-solute interactions may inhibit cross-slip by producing local curvatures in the dislocation line. Since a minimum length of straight dislocation is required before cross-slip can take place, local curvature in dislocation lines tends to inhibit cross-slip. The dislocation-solute interaction can be divided into the atomic size effect and the shear modulus effect [6,7]. The atomic size effect is proportional to $(1/a)(da/dc)$, where a is the lattice parameter of the solvent and c is the atomic fraction of the solute. The shear modulus effect is proportional to $(1/G)(dG/dc)$, where G is the shear modulus of the solvent.

The strains around most substitutional solute atoms may be represented by a misfitting-sphere-in-hole model. If the crystal is expanded by solute, it is supposed that the foreign atoms are larger than the ones they replace; hence they distort the lattice spherically just as would an elastic sphere forced into a spherical hole of smaller diameter in an elastic continuum. An idealized elastic continuum model is used to represent the effect of placing one particle in a crystal composed of other discrete particles. This model is brought back to reality by using a gross property of the crystal as a measure of the size of the solute atom. Thus oversized atoms will expand the lattice, and the rate of expansion $(1/a)(da/dc)$ is a measure of the fractional atomic radius by which a solute atom fails to fit the site it is forced into.

If a solute atom is represented by a small region not of different size but of different elastic properties from the matrix materials, a second interaction of equal importance occurs. In this case there is no preexisting lattice distortion; the effect of the solute arises only when the stress field of a dislocation is introduced. The interaction comes from the extra work which the dislocation must do as it approaches an elastically hard spot in the crystal (or extra work the dislocation must do while being pulled away from a soft spot). The macroscopic property which is used as a measure of the "atomic shear modulus" is the rate of change of modulus with concentration. This measure of modulus difference is given by $(1/G)(dG/dc)$.

Short-range order is a local lattice inhomogeneity which interacts elastically with dislocations to produce dislocation curvature, since the dislocation sees a variation in lattice friction as it moves [8]. The destruction of localized short-range order tends to make the passage of subsequent dislocation easier, thus resulting in planar slip.

In general a solid solution is not random. Some degree of local order (a local preponderance of like or unlike neighbors) exists. The energy of a solid solution varies linearly with the degree of local order whereas the entropy varies logarithmically; therefore,

unless the interaction between like and unlike neighbors is identical, the equilibrium state will have a nonzero local order. This order need not be very great to make a significant contribution to hardening.

Local order of the short-range-order type, in which there are more than the random number of unlike nearest neighbors, is not equivalent to a conglomeration of small regions of long-range order; also local order of the clustering type, in which the preponderance of like neighbors is high, is not equivalent to a number of small clusters of B atoms dispersed in a matrix of A. The nearest-neighbor local-order parameter is defined as $\alpha = 1 - P_{ab}/M_a$, where P_{ab} is the probability of finding a particular atom a as nearest neighbor to an atom b, and M_a is the mole fraction of a, which is the corresponding probability in a random solution. Beyond some critical value, which varies with composition and crystal structure, purely local order is not possible and a phase transformation occurs, either to a superlattice when attraction is between unlike atoms or to a two-phase structure when attraction is between like atoms.

Slip of one Burgers vector in a short-range-order structure reduces the number of unlike bonds to approximately the random number; further slip produces essentially no further change, because the atom positions are uncorrelated beyond nearest-neighbor distances. This reduction in the number of unlike bonds requires work, since unlike bonds are of lower energy in this instance. The situation is similar for clustering, where the number of like bonds across the slip plane is reduced to the random number, with a corresponding increase in energy. The effect can be treated quantitatively by counting the average number of bonds cut in any particular composition and crystal structure.

The phase diagram of the Ti-Al system is shown in Fig. 2. In the Ti-rich region this diagram from van Loo and Rieck [9] agrees remarkably well with the results of Blackburn [10]. Differences between this diagram and others are attributable to both the shape of the homogeneity regions and the slow diffusion process at temperatures below the transition point of Ti.

An investigation into the changes of stacking fault energy γ with increasing solute concentration in the binary Ti-Al alloy system appeared to be a logical and promising starting point. Usually γ is determined through transmission electron microscopy measurements of extended nodes, of fault pairs, of direct resolution of dissociated dislocations using weak beam techniques, and of stacking fault tetrahedra. However in pure Ti the nodes are not extended, the inference being that γ is too high to be measured directly. Other techniques for measuring γ indirectly include x-ray line broadening, τ_{III} mechanical measurements, texture measurements, and measurement of quenched stacking fault tetrahedra. Of these techniques the most promising and straightforward method is x-ray-line-broadening analysis, in which a quantity (the stacking fault probability) inversely proportional to γ can be deduced. X-ray-line-broadening analysis is based on the spreading of the diffraction line due to severe deformation of the specimen. This broadening is compared to the instrumental broadening obtained by the diffraction from a well-annealed powder. The resulting broadening can then be interpreted in terms of the microstrain, domain size, and stacking faults that occurred as a result of dislocation interactions during

the deformation process. These data can be complemented by transmission electron microscopy of both annealed and slightly deformed alloys.

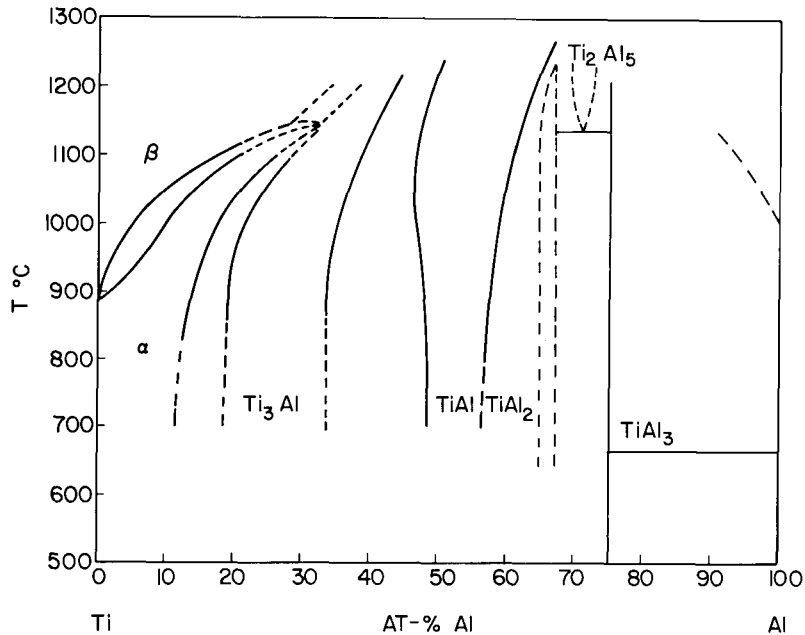


Fig. 2 — Phase diagram of Ti-Al according to van Loo and Rieck [9]

The initial work [1] showed that in the Ti-Al binary system the stacking fault probability varied exponentially with solute concentration (0 to 12 at-%) and that the dislocation arrangements in these alloys could be explained in terms of changes in stacking fault energy. The values of stacking fault probability were later independently confirmed by other workers [2].

X-RAY-LINE-BROADENING PROCEDURES

The alloys were prepared for x-ray diffraction by filing at room temperature, collecting the resulting small metal particles, and then sifting these particles through a No. 325 mesh sieve. The resulting powder was placed in a specimen holder using a dilute solution of collodion in amylacetate as a binder. X-ray line profiles of the $(10\bar{1}1)$, $(10\bar{1}2)$, and $(10\bar{1}3)$ fault-affected reflections, as well as the $(10\bar{1}0)$, (0002) , $(11\bar{2}0)$, and (0004) fault-unaffected reflections were recorded. The incident radiation was $CuK\alpha$; a nickel filter and both current and voltage regulators were employed. The diffracted intensities were incident on a LiF curved-crystal monochromator, then detected by a proportional counter; the resulting signal was amplified and processed through a pulse-height analyzer. The region $26^\circ \leq 2\theta \leq 90^\circ$ was step-scanned for a preset time of 100 seconds at steps of 0.02° . The high-purity well-annealed Ti sample used in the previous investiga-

tion was again employed as a standard. The x-ray line profiles from the standard were spread over a much narrower range of angles, and the intensity (peak) was much greater for every reflection than that of the cold-worked filings.

Higher-order peaks were not measured because of their diffuseness and considerable peak overlap. Those diffraction peaks in which tails overlapped were separated by assuming that the adjacent peak could be represented by a Cauchy distribution function and by subtracting the total intensity contributed by these tails from the experimental values [11].

FOURIER ANALYSIS

The x-ray diffraction line profiles were digitized and used as input to a computer program [12] which corrected the data for polarization and geometric factors, for atomic scattering factors, and for the $K\alpha$ -doublet by Keating's method [13]. The Fourier coefficients of the line profiles were evaluated using the technique of numerically calculating the trigonometric integrals proposed by Filon [14]. Each line profile from the deformed powders was corrected for errors from instrumental broadening by the technique of Stokes [15], which uses the profile of the corresponding peaks of annealed alloys; in this case pure Ti was the standard.

The corrected Fourier coefficients A_L of the fault-unaffected peaks, where A_L is the Fourier coefficient at a distance L normal to the reflecting plane, were separated into size coefficients A_L^S and distortion coefficients A_L^D , by computing the intercepts and slopes of the graphs of $\ln A_L$ versus $1/d^2$ for different values of $L = nd$, where d is the interplanar spacing of the reflection and n is the harmonic number. The slopes of these curves are proportional to the mean-square microstrains $\langle \epsilon^2 \rangle$, and the intercepts of these curves are the true particle size coefficients A_L^P . The true domain size and strain thus calculated were considered to be approximately the same as those for fault-affected reflections. These strain values were then used to determine the distortion coefficients for a Gaussian strain distribution

$$A_L^D = e^{-2\pi^2 L^2 \langle \epsilon^2 \rangle / d^2},$$

where $\langle \epsilon^2 \rangle$ is the mean-square microstrain in the crystal.

The size coefficients A_L^S for fault-affected reflections, having been corrected for strain broadening by the use of the distortion coefficients, include effects arising from particle size and faulting. The deformation fault probability α , the growth fault probability β , and the average domain size D are calculated from the slopes of the graphs of A_L^S versus L using the relations

$$-\frac{dA_L^S}{dL} = \frac{1}{D} + \frac{|\ell|d}{c^2} (3\alpha + 3\beta)$$

for the reflection $h - k = 3t \pm 1$ and ℓ even,

$$-\frac{dA_L^S}{dL} = \frac{1}{D} + \frac{\ell |d|}{c^2} (3\alpha + \beta)$$

for the reflections $h - k = 3t \pm 1$ and ℓ odd, and

$$-\frac{dA_L^P}{dL} = \frac{1}{D}$$

for the reflection $h - k = 3t$ or ℓ zero, where d is the interplanar spacing of the reflecting plane ($hkl\ell$), $c = 2d_{0002}$, and t is an integer. The growth fault probability is assumed to be negligibly small, since the reflections from the annealed powders are sharp [1, 2, 16-19].

EXPERIMENTAL RESULTS

The Fourier coefficients A_L of each x-ray line profile measured were corrected for instrumental broadening. The mean-square microstrain, which was determined from fault-unaffected reflections, was used to evaluate the size coefficients A_L^S for the fault-affected peaks from the Fourier coefficients A_L of these peaks. The initial slopes of the size coefficients, when corrected [20] for the curvature effects at small L values, are a measure of the domain size in the crystals. Thus the apparent domain sizes determined from the fault-affected peaks are smaller than the mean domain sizes measured from the fault-unaffected peaks.

The composition of each alloy, the mean domain size, the mean-square microstrain, and the stacking fault probability are summarized in Tables 1 through 4. The errors inherent in the measurement of the particle sizes are of the order of $\pm 10\%$. The microstrain values are the microstrains measured at $L = 50 \text{ \AA}$.

Table 1
 Stacking Fault Probabilities α
 in Cold-Worked Ti-O Alloys

Composition: O (wt-%)	$\langle e^2 \rangle \times 10^6$	D (\AA)	$\alpha \times 10^3$
0.01	4	230	2
0.12	8	260	3
0.3	19	210	8

Table 2
Stacking Fault Probabilities
in Cold-Worked Ti-Al-O

Composition: (wt-%)		$\langle \epsilon^2 \rangle \times 10^6$	D (Å)	$\alpha \times 10^3$
Al	O			
4.20	0.090	2	110	6
4.00	0.154	21	115	9
3.88	0.330	19	125	8
6.05	0.065	18	130	6
6.05	0.175	44	180	8
8.95	0.145	15	90	10
8.78	0.333	10	80	15

Table 3
Stacking Fault Probabilities in
Cold-Worked Ti-6Al-4V Alloys

Composition: O (wt-%)	$\langle \epsilon^2 \rangle \times 10^6$	D (Å)	$\alpha \times 10^3$
0.05	17	146	17
0.11	29	107	29
0.15	26	57	19

Table 4
Stacking Fault Probabilities in
Cold-Worked Commercial Ti Alloys

Alloy	$\langle \epsilon^2 \rangle \times 10^6$	D (Å)	$\alpha \times 10^3$
7Al-2Cb-1Ta	30	100	20
5Al-2.5Sn	19	60	39
7Al-12Zr	35	80	8
4Al-3Mo-1V	22	90	7

DISCUSSION

Most of the alloys examined are based at least partially on the Ti-Al system; hence Fig. 3 is included. Figure 3 is a plot of $\ln \alpha$ versus composition (c) for Ti-Al solid solutions and shows the agreement that is found between two experimenters using different methods of analysis. The agreement is quite good, especially at higher Al contents. For pure Ti the differences may be explained by either purity effects or to inaccuracies [21, 22] in the determination of α below 0.003. The accuracy in the measurement of α is limited to 0.001 [2]. Using this information as guidelines, let us discuss each alloy system examined.

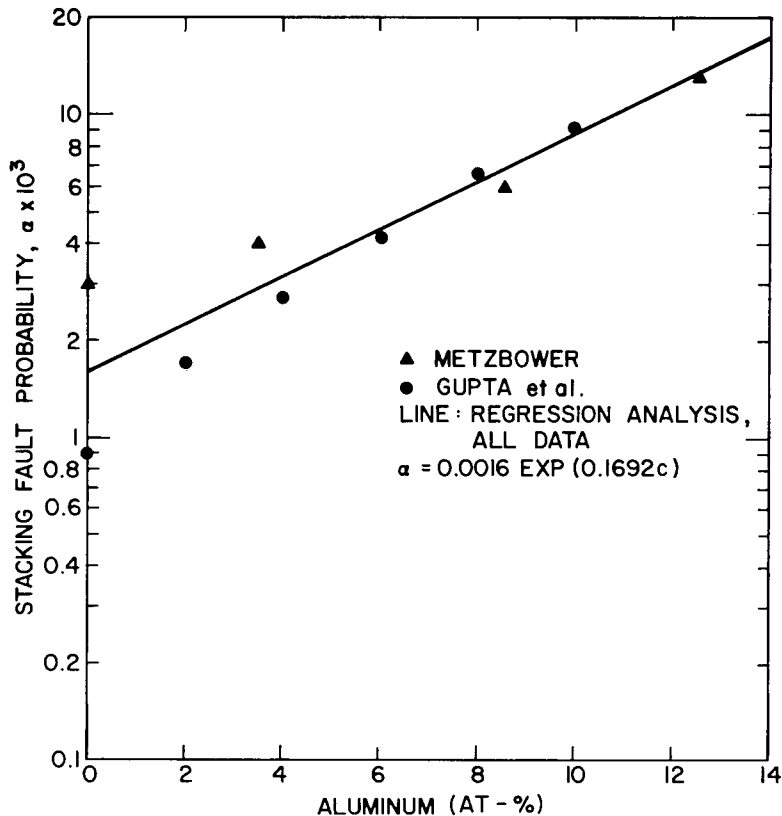


Fig. 3 — Stacking fault probability of Ti-Al as a function of Al content

Ti-O Alloys

Three grades of unalloyed Ti of varying purity were investigated. The high-purity grade was iodide titanium (IoTi), whereas the commercial purity grades were A50 and A70. The strain hardening behavior of these alloys by severe plastic deformation was studied extensively by Biswas [23]. The high-purity Ti shows the formation of dipoles and short dislocations leading to a cellular structure, whereas the commercial grades show long, straight, parallel screw dislocations in prism planes, becoming denser at higher strains. The difference in the two dislocation structures is attributed (a) to an increasing drag force, due to interstitial solutes, on the screw dislocations compared to edge dislocations, and (b) to an increasing difficulty of cross-slip arising from the higher friction stress and/or lower stacking fault energy. The cellular formation noted in the IoTi is explained by the generation of edge-dislocation dipoles and cross-slipping onto the basal planes and the subsequent interaction with moving dislocations.

Addressing the question on which planes (prism, basal, or pyramidal) the dislocations dissociate, Biswas deduces the dislocations can dissociate most favorably on basal planes, to a lesser extent on prism planes, and not at all on pyramidal planes. The dislocation segments which cross-slip into the basal plane most likely dissociate immediately after cross-slip, and in that case the partials must recombine again before they

cross-slip back onto prism plane for continued motion. Biswas believes that, since screw dislocations lie in the basal plane and edge dislocations lie normal to it, the screw dissociates into Shockley-type partials on the basal plane whereas an edge probably dissociates into $1/9$ $[11\bar{2}0]$ and $2/9$ $[11\bar{2}0]$ partials on the prism plane. The Shockley partials must coalesce before the screw moves onto the prism plane, and during subsequent motion the screw probably dissociates into $1/9$ $[11\bar{2}0]$ and $2/9$ $[11\bar{2}0]$ partials on the prism plane; this dissociation lowers the energy of the screw. Again, during the reverse cross-slip the screw dissociates into Shockley partials while it is on the basal plane.

Biswas concludes from the above considerations that both prism and basal-plane stacking faults will contribute to the stacking fault probability. Hence the fact that the stacking fault probability increases with increasing impurity content does not prove *conclusively* that the propensity to cross-slip decreases in the same way, because the increase in stacking fault probability could be due to a decrease in one or both of the two stacking fault energies. However, it is *likely* that an increase in stacking fault probability is due to a decrease in stacking fault energy on the basal and/or prism planes, so that double cross-slipping becomes increasingly difficult, leading to planar dislocation arrays instead of a cellular structure.

Sargent and Conrad [24] suggest a chemical interaction between Ti and O as the basis for the high degree of strengthening produced by O in the Ti lattice. Since the hardening cannot be explained simply in terms of elastic-strain-field interactions, they conclude that the stabilization of the α phase by O, the existence and formation of ordered structure, the abnormal resistivity, and the high activation energy for diffusion all suggest that O may be chemically bonded to Ti through the formation of a covalent bond. They also note that, assuming random distribution of the O impurities, more Ti-O bonds are found to cross the basal plane than to cross the first-order prism planes. In Ti, slip occurs easier in the prism planes.

Williams, Sommer, and Tung [25] explain why increasing O might cause a transition to planar glide in α Ti at low temperatures by the attractive suggestion that the ordering tendencies exhibited in more concentrated Ti-O solid solutions are preceded by short-range ordering in the more dilute solid solutions studied, thereby producing coplanar slip. Direct proof of short-range ordering (or lack thereof) is experimentally difficult, since O has a low scattering power for x-rays and electrons.

Ti-Al-O Alloys

The Ti-Al-O group of alloys can best be discussed by considering the effect of O on each of the Ti-Al alloys. Previous measurements on Ti-Al binary alloys have indicated that the stacking fault probability of a 4-wt-% alloy is 0.008, that of a 6-wt-% alloy is 0.011, and that of a 9-wt-% alloy is 0.021. Thus the stacking fault probability of the 4-wt-% alloy does not change with O content, the stacking fault probability of a 6-wt-% alloy is slightly lower than expected, and the stacking fault probability of a 9-wt-% alloy measure is only about half of the expected values. Thus, if influential at all, O tends to lower the stacking fault probability. However Al and O additions are reported [26] to act additively in increasing susceptibility to stress corrosion cracking. If this is so, no decrease in stacking fault

with O level would be observed. Oxygen has a deleterious effect on the binary Ti-Al alloys in that the Ti-4Al-0.33O alloy is susceptible. A Ti-6Al alloy is most likely susceptible, but certain β stabilizers and thermomechanical processing can make it nonsusceptible.

The effect of O then is not to act synergistically with Al in changing the stacking fault probability and the corresponding dislocation structures but to change the yield strength of the alloy through a dislocation-and-solute interaction.

Conrad [27] argues that the facts that the effect of Al on the strength of Ti is athermal, that the plot of stress versus Al content exhibits a positive curvature, and that dislocation pairs occurred at the head of planar arrays in Ti-Al alloys containing more than 10 at-% Al all suggest that the strengthening of Ti by Al may be due to the presence of short-range order. The decrease in strength for Al contents greater than 13 at-% is attributed to the occurrence of another strengthening mechanism (the clustering or precipitations of the Ti_3Al (α_2) phase), which may occur even though the alloys were water-quenched from the α -phase region. These calculations give an interaction energy (μ) of -0.078 eV, which in turn yields a local-order coefficient (α) of -0.085 for a Ti-10-at-% Al alloy.

Flinn [8] states that beyond some critical value purely local order is not possible and that the upper limit in the magnitude of α is not known in general but is about 0.2 for Cu_3Au systems and about 0.3 for β -brass systems. Comparing the value of α calculated from Conrad's data to these values, the question arises as to whether short-range order can completely explain the dislocation arrays.

Rosenberg and Nix [28] examined Ti-Al alloys with Al values ranging from 0 to 15 at-%. Using a heat treatment in the β phase field and then in the upper region of the $\alpha + \beta$ phase field, they found no evidence for the presence of Ti_3Al from either x-ray diffraction or selected-area electron diffraction. Great lengths of dislocations lying in or near screw orientation were observed in the Ti-Al alloys but not in the unalloyed Ti base. Slip was observed to proceed in tight slip bands. Slip on secondary slip systems was rare, because the textured polycrystalline specimens were oriented to favor prismatic slip. In the unalloyed materials, dislocations and cells readily developed with strain, but this was not true of the alloys containing more than 3 at-% Al. Evidently cross-slip is strongly inhibited in the alloys. Cross-slip is not precluded, however, since it was observed in the nominal Ti-15Al alloy. Their explanation for the coplanar arrays is based on a covalent directional bonding between Ti and Al, which implies a high Peierls stress such that dislocations would tend to lie along close-packed directions in order to minimize their line energies.

Ti-6Al-4V -- Oxygen Alloys

The Ti alloy 6Al-4V is an $\alpha - \beta$ alloy. The mechanical properties of the alloy can be varied by changing the forging conditions and subsequent hot rolling temperatures. The alloy can be forged in either the $\alpha + \beta$ phase field or the β phase field. Subsequent rolling temperatures can easily be varied between the forging temperatures. Three alloys with different O levels were examined. All of the alloys had undergone thermomechanical processing in the form of forging in the β region starting at 2100°F (1149°C). The final

rolling temperature was 1900°F (1038°C). In general, over the entire range of thermomechanical processing the yield strength increases with increasing O level whereas the fast fracture resistance (as measured by the Dynamic Tear Test) and the resistance to stress corrosion cracking decreases with increasing O levels. In the particular case of the alloys selected for x-ray-line-broadening analysis, the yield strength increased from 106.6 ksi at 0.05 wt-% O to 121.4 ksi at 0.11 wt-% O and slightly decreased to 119.2 ksi at 0.15 wt-% O [29]. The stacking fault probability of these alloys went from 0.017 at 0.05 wt-% O to 0.029 at 0.11 wt-% O to 0.019 at 0.15 wt-% O. While the trend between yield strength and stacking fault probability with increasing O level is the same, there is no parallelism: the magnitude of the increase in stacking fault probability and yield strength in going from 0.05 to 0.11 wt-% O does not correspond to the magnitude of the decrease in going from 0.11 to 0.15 wt-% O.

Commercial Ti Alloys

Because of the correlation that exists between stacking fault probability and resistance to stress corrosion cracking in Ti-Al binary alloys, x-ray-line-broadening analysis was done on four commercial alloys. Two of these alloys (4Al-3Mo-1V and 7Al-12Zr) are considered to be resistant to stress corrosion cracking [30, 31], whereas the other two alloys (7Al-2Cb-1Ta and 5Al-2.5Sn) are considered to be susceptible to stress corrosion cracking [30, 32]. The 4Al-3Mo-1V alloy is an $\alpha + \beta$ alloy, and the Al content is low enough so that the dislocation arrangement is mostly cellular. The 7Al-12Zr alloy is an α alloy, and although the Al content is high, the addition of Zr possibly reduces susceptibility (increases resistance) to stress corrosion cracking. Indeed the stacking fault probability of a Ti-7Al alloy is approximately 0.012, whereas the stacking fault probability of the Ti-7Al-12Zr is measured at 0.008. On the other hand the effect of Sn generally decreases the resistance to stress corrosion cracking. The Ti-5Al-2.5Zn alloy has a stacking fault probability of 0.039, whereas the Ti-5Al alloy would be expected to have a stacking fault probability of 0.006. The 7Al-2Cb-1Ta alloy is an $\alpha + \beta$ alloy in which the Al content is high enough so that the dislocations arrays are coplanar. Its stacking fault probability is 0.020, whereas a Ti-7Al alloy would be expected to have a stacking fault probability of 0.012.

Zr and Sn are substitutional elements that cannot be classified definitely as α or β stabilizers. They are used in commercial alloys as substitutional α stabilizers. However, Zr appears to negate to a certain extent the effect of Al, whereas Sn appears to enhance greatly the effect of Al. If Al, Zr, and Sn acted with the same power in stabilizing the α phase of Ti, the Ti-7Al-12Zr alloy would be expected to have a high stacking fault probability, a coplanar dislocation arrangement, and a short-range order evidenced by the formation of Ti_3 (Al + Zr). On the other hand the Ti-5Al-2.5Sn alloy would be expected to have a stacking fault probability similar to a Ti-8Al alloy. Thus Sn is a much greater alpha stabilizer than Al. Zr when combined with Al appears to negate the effect of Al to a great extent, as evidenced by the stacking fault probability of the Ti-7Al alloy (0.012) in comparison with that of the Ti-7Al-12Zr alloy (0.008).

CONCLUSIONS

In conclusion:

- The increase in stacking fault probability in titanium-oxygen alloys can explain the morphology of the dislocation arrays in these alloys.
- The effect of oxygen in titanium-aluminum alloys is not synergistic in changing the stacking fault probability and the corresponding dislocation structures.
- No correlation is evident between oxygen concentration and susceptibility to stress corrosion cracking in the 6Al-4V alloys.
- The four commercial alloys examined show a correlation between stacking fault probability and susceptibility to stress corrosion cracking.
- The alloying effects of aluminum and/or oxygen in the dislocation arrangements of titanium is still not completely certain. Short-range order and stacking fault probability definitely play important roles in controlling the dislocation structures; dislocation-solute reactions may be the operative mechanism by which oxygen influences alloy behavior.

REFERENCES

1. E.A. Metzbower, *Met. Trans.* **2**, 3099 (1971).
2. R.K. Gupta et al., *Z. Metallk.* **63**, 575 (1972).
3. P.R. Swann, p. 31 in *Electron Microscopy and Strength of Crystals*, G. Thomas and J. Washburn, editors, Interscience, New York, 1963.
4. Y. Nakada and T.C. Tisone, *Second Conference on Strength of Metals*, Vol. 1, 1970, pp. 288-299.
5. P.G. Partridge, *Metallurgical Reviews*, pp. 169-194.
6. R.L. Fleischer and W.R. Hibbard, Jr., *The Relation Between the Structure and Mechanical Properties of Metals*, HMSO, London, 1963, p. 262.
7. R.L. Fleischer, pp. 93-140 in *The Strengthening of Metals*, D. Peckner, editor, Reinhold, New York, 1964.
8. P.A. Flinn, pp. 17-50 in *Strengthening Mechanisms in Solids*, ASM, Metals Park, Ohio, 1962.
9. F.J.J van Loo and G.D. Rieck, *Acta Met.* **21** (1), 73-84 (Jan. 1973).
10. M.J. Blackburn, *Trans. Met. AIME* **239**, 1200 (1967).
11. S. Sato, *Japanese J. Appl Physics* **1**, 210 (1962).
12. E.A. Metzbower, "Computer Programs for the Analysis of the Broadening of X-ray Powder Patterns," NRL Report 7253, Apr. 1971.
13. D.T. Keating, *Rev. Sci, Instr.* **30**, 725 (1959).

14. L.N.G. Filon, Proc. Roy. Soc., Edinburgh, 44, 38 (1928-1929).
15. A.R. Stokes, Proc. Phys. Soc., London, 61, 382 (1948).
16. M. De and S. Sen, Brit. J. Appl. Phys. (J. Physics D) 1, 1141 (1968).
17. S.P. Sen Gupta and K.N. Goswami, Brit. J. Appl. Phys. 18, 193 (1967).
18. R.P. Stratton and W.J. Kitchingman, Brit. J. Appl. Phys. 16, 1311 (1965).
19. R.P. Stratton and W.J. Kitchingman, Brit. J. Appl. Phys. 17, 1039 (1966).
20. R.L. Rothman and J.B. Cohen, Advan. X-Ray Anal. 12, 208 (1968), published 1969.
21. S. Lele and T.R. Anantharaman, Z. Metallk. 58, 461 (1967).
22. R.K. Gupta, T.K.G. Namboodri, and P.R. Rao, Proc. Sym. Material Sci. Res., India, 1970, p. 479.
23. C.P. Biswas, Ph.D. Dissertation, MIT, Jan. 1973.
24. G.A. Sargent and H. Conrad, Scripta Met. 6, 1099-1101 (1972).
25. J.C. Williams, A.W. Sommer, and P.P. Tung, Met. Trans. 3, 2979-2984 (Nov. 1972).
26. S.R. Seagle, R.R. Seeley, and G.S. Hall, ASTM STP 432, p. 170, 1968.
27. H. Conrad, Scripta Met. 7, 509-512 (1973).
28. H.W. Rosenberg and W.D. Nix, Met. Trans. 4, 1333-1338 (May 1973).
29. R.W. Judy, Jr., R.J. Goode, and R.W. Huber, "Oxygen Level and Processing Effects on Strength and Fracture Resistance of Ti-6Al-4V," NRL Memorandum Report 2121, May 1970.
30. R.E. Curtis, R.R. Boyer, and J.C. Williams, Trans. ASM 62, 457 (1969).
31. M.J. Blackburn, J.A. Feeney, and T.R. Beck, "State-of-the-Art-of-Stress-Corrosion-Cracking of Titanium Alloys," Part 4, June 1970 (Boeing technical report for the ARPA Coupling Program on Corrosion; ARPA Order 878).
32. B.F. Brown, T.J. Lennox, R.L. Newbegin, M.H. Peterson, J.A. Smith, and L.J. Waldron, "Marine Corrosion Studies — Deep Ocean Technology, Stress Corrosion Cracking, Cathodic Protection — Second Interim Report of Progress," NRL Memorandum Report 1574, Nov. 1964.

